Feedback Linearization Of Direct-Drive Synchronous Wind-Turbines Via a Sliding Mode Approach

José Matas, Miguel Castilla, Josep M. Guerrero, *Member, IEEE*, Luis García de Vicuña, and Jaume Miret, *Member, IEEE*

***Abstract*—As the grid code specifies, wind turbines have to remain connected to the grid at voltage levels far below the nominal values. The improvement of wind turbine performance under such conditions has become a problem of general concern. However, this performance usually relies on conventional linear controllers that operate at network faults far off the nominal point for which they were designed. As a consequence, wind turbines should operate with increasing converter currents, which may result in converter damage. This paper proposes a nonlinear controller for converter-based wind turbines that ensures that the currents are maintained within the design limits. The controller is based on feedback linearization theory and is applied to the system through a sliding mode approach. This controller is robust against system perturbations and uncertainties, and overcomes the usually complex implementation that is associated with feedback linearization controllers.**

***Index Terms*—Feedback linearization, grid fault, ride-through control, sliding mode control, wind energy, wind power generation.**

I. Introduction

WIND power is one of the most cost-effective systems available today to generate electricity from renewable sources. For this reason, wind energy is being widely used to reduce the levels of polluting CO_2 emissions. In the case of high power ratings, variable speed wind turbines are usually applied due to cleaner power delivery to the grid, higher capacity to extract energy from the wind, lower noise at low wind speeds, lower drive train torque, and control flexibility. The most common variable speed wind turbines are the doubly fed induction generators (DFIG) and direct driven synchronous generators (DDSG). DFIGs utilize a transmission gearbox to connect the rotor of the wind turbine to the generator. In contrast, DDSGs are directly coupled to the wind turbine, eliminating the gearbox, simplifying the power plant, and improving efficiency at lower wind speeds [1], [2].

As the level of wind energy penetration in the electrical power systems increases, several grid connection codes have been introduced to ensure network power quality. These codes define the operation boundary for a wind turbine connected to the grid in terms of power factor, frequency range, voltage tolerance, and fault ride-through capability. Today, wind turbines are required to remain connected to the grid during network disturbances and cannot be simply disconnected from the grid as in the past [3], [4]. Among these disturbances, voltage dips have a great impact on wind turbines since the output current of the generator increases significantly and can easily damage the system equipment. Thus, in compliance with grid codes, wind turbines should be able to override the large currents caused by temporary voltage dips, and to continue feeding in current during a grid short circuit. From a functional point of view, this means that wind turbines have to behave like conventional power plants.

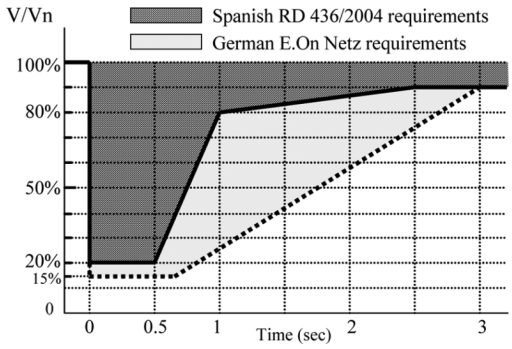

Fig. 1. Spanish RD 436/2004 and E.On Netz fault ride-through requirements for wind farms.

In 2004, the Spanish Royal Decree RD 436/2004 established the transmission grid codes and the fault ride-through specifications for wind farms in Spain (see Fig. 1) [5]. The German E.On Netz grid code is also shown in this figure as a heavy dotted line. This figure shows how wind turbines are allowed to disconnect from the grid only when the grid voltage goes below the curve plotted by the heavy lines (in time length or in voltage level). Note that the Spanish ride-through specification is less restrictive than the E.On netz by only 5% of the maximum allowable voltage dip level, but even less restrictive in time length duration.

In a standard DFIG and DDSG, a back-to-back voltage source converter (VSC) with a dc-link is normally used. In DFIGs, the power is supplied by the generator stator to the grid and, at the same time, electric power is exchanged with the grid via the VSCs connected between the grid and the rotor circuit. In this situation, the converter handles only a portion of the generator's output power (about one third of the nominal power), which results in converter size and cost savings. Unfortunately, the converter is very sensitive to transient current surges caused by faults in the network and special care must be

Manuscript received September 6, 2007; revised December 11, 2007. This work was supported by the Spanish Ministry of Science and Technology under Grant ENE2006-15521-C03-01. Recommended for publication by Associate Editor Z. Chen.

J. Matas, M. Castilla, L. García de Vicuña, and J. Miret are with the Department of Electronic Engineering, Technical University of Catalonia, Barcelona 08800, Spain (e-mail: matas@eel.upc.edu; matasalc@gmail.com).

J. M. Guerrero is with the Department of Automatic Control Systems and Computer Engineering, Technical University of Catalonia, Barcelona 08036, Spain.

Digital Object Identifier 10.1109/TPEL.2008.921192

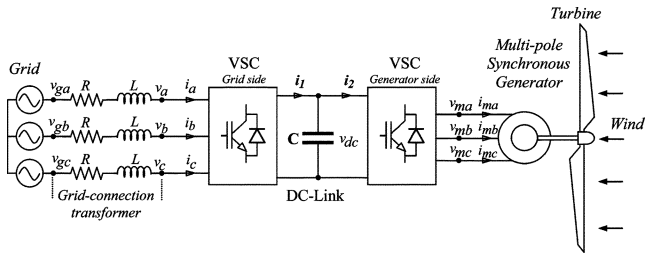

Fig. 2. Direct drive synchronous generator connected to the grid via back-to-back VSCs.

taken to avoid component damage [6], [7]. For DDSGs, in order to allow variable speed operation, the generator is connected to the grid through a back-to-back VSC that acts as a frequency converter and decouples the generator from the grid, see Fig. 2. Consequently, the fault ride-through capability of the wind turbine depends on the converter control. The converter can limit the current to rated values during dips, and continue to deliver power and reactive power at reduced voltage levels. Therefore, in the event of a fault, these turbines could stay connected to the grid and may help the conventional power stations rebuild the voltage after grid failures [8]–[12].

Several studies of the behavior of different types of turbines during faults have been conducted [13]–[21]. In [17], a control strategy is proposed to improve the fault ride-through capability of DFIG wind turbines. This strategy consists in reducing the time that it takes to restore the turbine pre-fault condition after the fault is cleared, which prevents voltage collapse during the restarting process. [18] studies the steady-state voltage profile and the voltage ride-through capabilities of the induction generator-based wind farms with different reactive compensation techniques. In [19], a ride-through solution for DFIGs is proposed which is based on limiting the high current in the rotor by providing a bypass for this current via a set of resistors that are connected to the rotor windings. With this solution, the synchronism of operation remains established during and after the fault and the wind turbine can survive grid faults without disconnecting from the grid. The effects of voltage dips on the controller's performance of DDSGs under unbalanced conditions have been studied in [6]. This work focuses on the PI control of the dc-link using current feed-forward, but does not consider the controller impact on the converter currents. In [20], a flexible active power control based on a fast current controller and a reconfigurable reference current is proposed to overcome grid faults on a distributed power system. In [21], a nonlinear controller based on feedback linearization theory is proposed for DDSGs. This controller improves the behavior of the conventional linear current controllers, keeping the current levels within their design limits, even for the stronger voltage dips set by actual grid codes. Moreover, the study shows how the converter currents can exceed the design limits due to the poor behavior of standard PI-based controllers, which operate far below their nominal operating point. However, the implementation of this approach is very complex due to the fact that it involves too many sensing variables and difficult mathematical operations having to do with the nonlinear controller conception.

This paper also proposes a nonlinear controller based on feedback linearization theory for DDSGs. However, the feedback linearization is applied through a sliding mode control approach, which avoids those complex calculations, uses few sensing variables, and simplifies further the controller structure. Furthermore, the sliding mode control employs a low pass filter on the switching function in order to reduce the chattering produced by the sliding motion in the system state variables. This filter reduces the chattering of the wind turbine to acceptable levels without affecting the performance of the controller. Several simulations are carried out in order to demonstrate the feasibility of this control approach. The reported results show an excellent behavior for this controller, which achieves faster response and lower dc-link current and voltage overshoots than the conventional linear PI controllers. These results also show how a proper dynamic response can be imposed on the system by the proper choice of the sliding surface coefficients. Additionally, several simulations are also performed to prove the controller robustness in the presence of model mismatches. The obtained results show that the controller has high robustness against parametric uncertainty and that these mismatches have a small impact on the controller behavior.

This paper is organized as follows. In Section II, the design of conventional PI linear controllers for DDSGs is briefly reviewed. In Section III, the feedback linearization theory is explained and its application to a DDSGs wind turbine is presented. The limitations of this approach are also outlined. In Section IV, an input–output feedback linearization controller based on sliding mode control is synthesized. Section V shows simulation results of the proposed sliding-mode nonlinear controller. Section VI presents the conclusions of this work.

II. Conventional Grid-Side VSC Control for DDSGs

Fig. 2 shows a detailed scheme for the connection of a DDSG to the grid using back-to-back VSCs. The generator-side VSC generates the voltage-phasor and the electric frequency at the generator terminals, which correspond to the desirable rotational speed of the wind turbine. Therefore, in order to achieve a precise speed control of the generator, it is crucial to obtain a constant dc-link voltage. For this reason, it is important to achieve an accurate power balance at both sides of the back-to-back frequency converter.

In normal operation, the generator-side VSC absorbs only the electric power produced by the multi-pole synchronous generator and this power is delivered to the grid via the dc-link and the grid-side VSC. In addition, considering that the dc-link and the back-to-back VSCs decouple the turbine generator from the ac-grid, the control system of the grid-side VSC can be conceived as a way to regulate the electric power transferred from the wind turbine to the grid.

In order to achieve a constant dc-link voltage most commercial wind turbines vary the level of active power injected to the grid. To do this, the system control of the grid-side VSC is designed to ensure that the current i_1 matches the current i_2, as closely as possible, see Fig. 2. The current i_2 is delivered by the generator-side VSC and is a function of the wind speed and generator torque. The mismatches between these currents will lead to variations in the dc-link voltage that can influence the system performance.

A. Current Control

If balanced conditions are assumed and using the Park transformation, the system equations that describe the operation of the grid side of the frequency converter can be expressed in the dq reference frame [16] as

$$v_{gd} - v_d = Ri_d + L\frac{di_d}{dt} - L\omega i_q \tag{1}$$

$$v_{gq} - v_q = Ri_q + L\frac{di_q}{dt} + L\omega i_d \tag{2}$$

where R and L represent the total resistance and inductance between the grid-connected transformer and the grid-side VSC. These equations can be rewritten as

$$L\frac{di_d}{dt} + Ri_d = v_{gd} - v_d + L\omega i_q = v_{RLd} \tag{3}$$

$$L\frac{di_q}{dt} + Ri_q = v_{gq} - v_q - L\omega i_d = v_{RLq}. \tag{4}$$

Now, a proportional-integral (PI) controller can be realized for each component with the following form:

$$v_{RLd} = k_p e_d + k_i \int e_d d\tau \tag{5}$$

$$v_{RLq} = k_p e_q + k_i \int e_q d\tau \tag{6}$$

where k_p is the proportional gain, k_i is the integral gain, and $e_d = i_d^* - i_d$ and $e_q = i_q^* - i_q$ are the errors derived from the reference currents. Therefore, substituting (5) in (3) and (6) in (4), the reference voltages of the grid-side VSC can be stated as

$$v_d = v_{gd} + L\omega i_q - k_p e_d - k_i \int e_d d\tau \tag{8}$$

$$v_q = v_{gq} - L\omega i_d - k_p e_q - k_i \int e_q d\tau. \tag{9}$$

These final relations allow the control system to regulate electric power around the desired references.

B. DC-Link Control

The dc-link controller can be derived from the analysis of the power balance between the ac and dc sides of the grid-side VSC [22], which is given by

$$v_{\rm dc} i_1 = \frac{3}{2}\left(v_{gd} i_d + v_{gq} i_q\right). \tag{10}$$

Here, the term v_{gq} can be taken as zero if correct alignment of the reference frame is considered. Thus, the following equation can be formulated if current i_2 is considered

$$C\frac{dv_{\rm dc}}{dt} = \frac{3}{2v_{\rm dc}}(v_{gd} i_d) - i_2 = f(v_{\rm dc}, v_{gd}, i_d, i_2). \tag{11}$$

As can be seen, this is a nonlinear equation. To derive the dc-link voltage controller, this relation can be linearized around a chosen operating point o as follows:

$$\frac{d}{dt}\Delta v_{\rm dc} = \left.\frac{df}{dv_{\rm dc}}\right|_o \Delta v_{\rm dc} + \left.\frac{df}{dv_{gd}}\right|_o \Delta v_{gd} + \left.\frac{df}{di_d}\right|_o \Delta i_d + \left.\frac{df}{di_2}\right|_o \Delta i_2 \tag{12}$$

which yields

$$C\frac{d\Delta v_{\rm dc}}{dt} = -\frac{3 i_{do} v_{gdo}}{2 v_{\rm dco}^2}\Delta v_{\rm dc} + \frac{3 i_{do}}{2 v_{\rm dco}}\Delta v_{gd} + \frac{3 v_{gdo}}{2 v_{\rm dco}}\Delta i_d - \Delta i_{2o} \tag{13}$$

where $v_{\rm dco}, v_{gdo}, i_{do}$, and i_{2o} are the operating point values, and Δ denotes incremental values [23]. Now, a PI dc-link controller can be applied to maintain a constant voltage

$$i_d^* = k_{pdc}(v_{\rm dc}^* - v_{\rm dc}) + k_{idc}\int (v_{\rm dc}^* - v_{\rm dc}) d\tau \tag{14}$$

where k_{pdc} and k_{idc} are the proportional and integral gains, respectively, and $v_{\rm dc}^*$ is the desired constant dc-link value.

C. Simulation Results

As in [21], a 1 MW variable-speed wind turbine is considered. The transformer is rated at 1.2 MVA and is conceived to step-up a voltage of 690 V to a grid voltage of 110 kV. The transformer has been modeled by an ideal transformer with a series resistor R and inductance L at the low side of the transformer, see Fig. 2, with values $R = 1.98$ mΩ and $L = 63.1$ μH. For the dc-link, a capacitor value of $C = 134$ mF is used [24]. The operating point for the dc-link capacitor is $v_{\rm dco} = 1050$ V while for the grid voltage at the transformer's low side it is $v_{gdo} = 690$ V, which corresponds to a direct component current of $i_{do} = 966$ A deduced from (10). The PI control parameters have been designed using root locus methods that lead to the following gains: $k_p = 0.1$ and $k_i = 3$ for the PI current controllers and $k_{pdc} = 50$ and $k_{idc} = 5000$ for the dc-link voltage PI controller.

These PI controllers are connected to the nonlinear model of the grid-side VSC [constituted by (1), (2), and (11)]. In order to evaluate the performance of the designed controllers under normal and fault conditions, a series of voltage dips on the grid were performed in the range of 100% to 15% of the nominal specified by the grid code (Fig. 1) and with a perturbation of -1000 A on the i_2 dc-link current. This current perturbation corresponds to the maximum expected change in the link current for this drive rating. The voltage dips were maintained at the specified level for a 200 ms test.

Fig. 3 shows how a sudden step perturbation in the dc-link i_2 current causes strong deviations in the dc-link capacitor voltage [Fig. 3(b)] which the controller tries to compensate for by increasing the current flowing to the grid [Fig. 3(a)]. As the grid voltage level decreases from its nominal value the response of the wind turbine deteriorates significantly. For a network voltage of 15% nominal, the produced transients reach about -1400 A for i_1 and 1115 V for $v_{\rm dc}$. Fig. 4 shows the peak grid-side VSC i_d current, which is plotted in pu. As in Fig. 3(a), an increase in the grid current is produced as the grid voltage dips reach lower values of nominal grid.

This performance is caused by the linear nature of the PI controllers that were designed around a small operating point. These controllers are working far off the nominal point of operation for which they were designed, because currently wind turbines must stay connected to the grid at voltages far below the nominal values. Moreover, the increasing current levels in the VSC during the network faults may result in damage to the power devices. Consequently, the control approach has to be improved

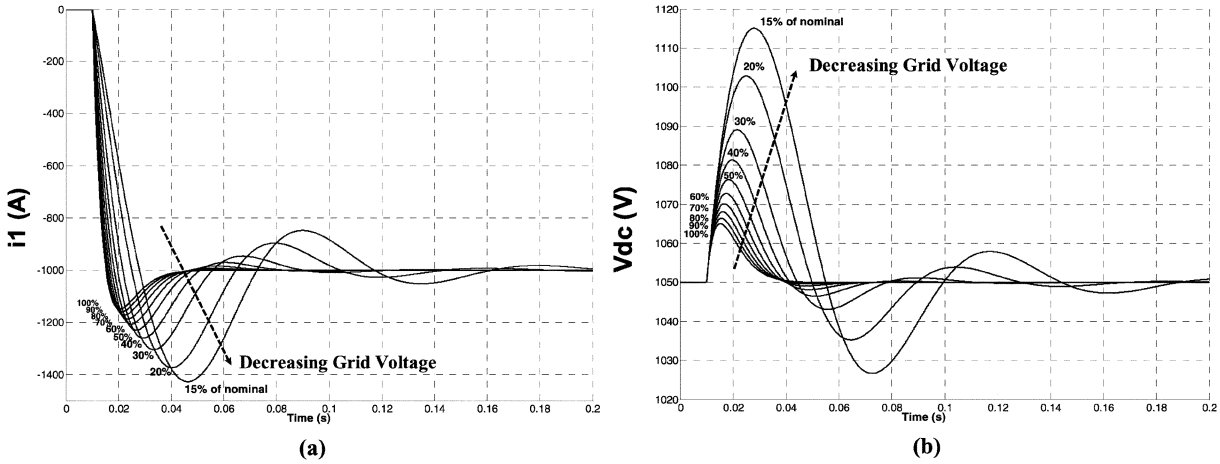

Fig. 3. Response to a -1000 A perturbation in the i_2 dc-link current to decreasing levels of grid voltage (from 100% to 15% nominal): (a) dc-link current i_1 and (b) dc-link capacitor voltage $v_{\rm dc}$.

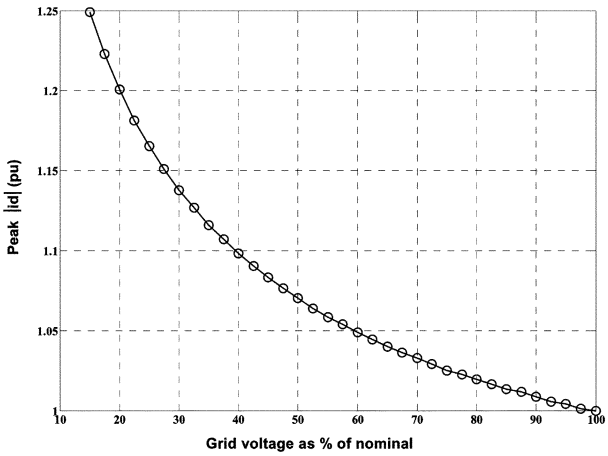

Fig. 4. Peak i_d magnitude response to a -1000 A perturbation in the i_2 dc-link current and for decreasing levels of grid voltage (from 100% to 15% nominal).

in order to ensure that the wind turbine current levels remain within their design boundaries.

III. Input–Output Feedback Linearization

A. Basic Concepts

The main idea behind feedback linearization is the reworking of the nonlinear system by means of a transformation and feedback in order to be able to obtain a linear relation between the input and output of the system [25]. Thus, feedback linearization tries to cancel the system nonlinearities through the input of the system. After that, a desired dynamic can be imposed on the system by adding a new control input.

Consider a multi-input multi-output (MIMO) nonlinear system with m inputs and m outputs

$$\begin{aligned}\dot{x} &= f(x) + \sum_{i=1}^{m} g_i(x)\cdot u_i \\ y_1 &= h_1(x) \\ &\cdots \\ y_m &= h_m(x)\end{aligned} \tag{15}$$

where $f(x)$, $g_1(x),\ldots,g_m(x)$ are smooth vector fields and $h_1(x),\ldots,h_m(x)$ are continuous functions on R^n. In nonlinear control the relative degree is an important theoretical concept, which is related to the number of times that the system outputs y_i have to be differentiated until the inputs u_i explicitly appear in the expression. Thus, assuming that r_i is the smallest integer such that at least one of the inputs explicitly appears in

$$y_i^{(r_i)} = L_f^{r_i} h_i + \sum_{j=1}^{m} L_{g_j} L_f^{r_i-1} h_i u_j \tag{16}$$

where $L_{g_j} L_f^{r_i-1} h_i(x) \neq 0$ for at least one j. Performing this process for each output y_i yields

$$\begin{pmatrix} y_1^{(r_1)} \\ \cdots \\ y_m^{(r_m)} \end{pmatrix} = \begin{pmatrix} L_f^{r_1} h_1 \\ \cdots \\ L_f^{r_m} h_m \end{pmatrix} + D \cdot \begin{pmatrix} u_1 \\ \cdots \\ u_m \end{pmatrix} \tag{17}$$

where $\boldsymbol{D}$ is an $m \times m$ matrix of the form

$$D = \begin{pmatrix} L_{g_1} L_f^{r_1-1} h_1 & \cdots & L_{g_m} L_f^{r_1-1} h_1 \\ \cdots & \cdots & \cdots \\ L_{g_1} L_f^{r_m-1} h_m & \cdots & L_{g_m} L_f^{r_m-1} h_m \end{pmatrix}. \tag{18}$$

If $\boldsymbol{D}$ is invertible, then a transformation can be made to input–output linearize the system by

$$u = D^{-1} \begin{pmatrix} \gamma_1 - L_f^{r_1} h_1 \\ \cdots \\ \gamma_m - L_f^{r_m} h_m \end{pmatrix} \tag{19}$$

where γ_i are the new inputs of the system. Now the input–output relations are given by

$$y_i = \gamma_i. \tag{20}$$

At this point, desired dynamics can be imposed on the system by the new system inputs.

B. Application to a DDSG Wind Turbine

The system model defined by (1), (2) and (11) can be expressed in matrix form as

$$\begin{pmatrix} \frac{d}{dt}i_d \\ \frac{d}{dt}i_q \\ \frac{d}{dt}v_{\rm dc} \end{pmatrix} = \begin{pmatrix} \frac{v_{gd}}{L} - \frac{R}{L}i_d + \omega i_q \\ \frac{v_{gq}}{L} - \frac{R}{L}i_q - \omega i_d \\ \frac{3}{2Cv_{\rm dc}}(v_{gd}i_d) - \frac{1}{C}i_2 \end{pmatrix} + \begin{pmatrix} 0 \\ -\frac{1}{L} \\ 0 \end{pmatrix} v_q + \begin{pmatrix} -\frac{1}{L} \\ 0 \\ 0 \end{pmatrix} v_d. \quad (21)$$

For convenience, we take the state variables i_q and $v_{\rm dc}$ as the outputs of the system

$$\begin{aligned} y_1 &= h_1(x) = i_q \\ y_2 &= h_2(x) = v_{\rm dc}. \end{aligned} \quad (22)$$

Now, differentiating the output y_1 with respect to time

$$\begin{aligned} \dot{y}_1 &= L_f h_1 + (L_{g_1}h_1)u_1 + (L_{g_2}h_1)u_2 \\ &= \frac{d}{dt}i_q = \frac{v_{gq}}{L} - \frac{R}{L}i_q - \omega i_d - \frac{1}{L}u_1 \end{aligned} \quad (23)$$

where $(L_{g_2}h_1) = 0$ and $u_1 = v_q$. Then, the relative degree value for this output is $r_1 = 1$. For the output y_2, the first and second-order time derivatives are

$$\begin{aligned} \dot{y}_2 &= L_f h_2 + (L_{g_1}h_2)u_1 + (L_{g_2}h_2)u_2 \\ &= \dot{v}_{\rm dc} = \frac{3}{2Cv_{\rm dc}}(v_{gd}i_d) - \frac{1}{C}i_2 \end{aligned} \quad (24)$$

$$\begin{aligned} \ddot{y}_2 &= L_f(L_f h_2) + L_{g_1}(L_f h_2)u_1 + L_{g_2}(L_f h_2)u_2 \\ &= \frac{3v_{gd}}{2Cv_{\rm dc}}\left(\frac{v_{gd}}{L} - \frac{R}{L}i_d + \omega i_q - \frac{1}{L}u_2\right) \\ &\quad - \frac{3i_d v_{gd}}{2Cv_{\rm dc}^2}\left(\frac{3(v_{gd}i_d)}{2Cv_{\rm dc}} - \frac{i_2}{C}\right) - \frac{1}{C}\dot{i}_2 \end{aligned} \quad (25)$$

where $(L_{g_1}h_2) = 0$, $(L_{g_2}h_2) = 0$, $L_{g_1}(L_f h_2) = 0$, and $u_2 = v_d$. For this output the relative degree is $r_2 = 2$. The vector relative degree of the system is $\boldsymbol{r} = (r_1, r_2) = (1, 2)$. Now, these equations can be rewritten in matrix form

$$\begin{pmatrix} \dot{y}_1 \\ \ddot{y}_2 \end{pmatrix} = \begin{pmatrix} A_1 \\ A_2 \end{pmatrix} + D\begin{pmatrix} u_1 \\ u_2 \end{pmatrix} \quad (26)$$

where

$$A_1 = \frac{1}{L}v_{gq} - \frac{R}{L}i_q - \omega i_d \quad (27)$$

$$A_2 = \frac{3v_{gd}}{2Cv_{\rm dc}}\left(\frac{v_{gd}}{L} - \frac{R}{L}i_d + \omega i_q\right) - \frac{3i_d v_{gd}}{2Cv_{\rm dc}^2}\left(\frac{3(v_{gd}i_d)}{2Cv_{\rm dc}} - \frac{i_2}{C}\right) - \frac{1}{C}\dot{i}_2 \quad (28)$$

$$\mathrm{D} = \begin{pmatrix} -\frac{1}{L} & 0 \\ 0 & -\frac{3v_{gd}}{2LCv_{\rm dc}} \end{pmatrix}. \quad (29)$$

The inverse of matrix $\boldsymbol{D}$ is

$$D^{-1} = \begin{pmatrix} -L & 0 \\ 0 & -\frac{2LCv_{\rm dc}}{3v_{gd}} \end{pmatrix} \quad (30)$$

which is nonsingular since

$$\det(D) = \frac{3v_{gd}}{2L^2Cv_{\rm dc}} \neq 0. \quad (31)$$

Therefore, the control law can be given by

$$\begin{pmatrix} u_1 \\ u_2 \end{pmatrix} = D^{-1}\left(-\begin{pmatrix} A_1 \\ A_2 \end{pmatrix} + \begin{pmatrix} \gamma_1 \\ \gamma_2 \end{pmatrix}\right) \quad (32)$$

which lead to the following input–output relation between the outputs y_i and the new inputs γ_i

$$\begin{pmatrix} \dot{y}_1 \\ \ddot{y}_2 \end{pmatrix} = \begin{pmatrix} \gamma_1 \\ \gamma_2 \end{pmatrix}. \quad (33)$$

At this point, taking into account that $\boldsymbol{r} = (1, 2)$, a desired dynamic response can be imposed to the system by choosing

$$\gamma_1 = \dot{y}_1^* + \lambda_{10}(y_1^* - y_1) \quad (34)$$

$$\gamma_2 = \ddot{y}_2^* + \lambda_{21}(\dot{y}_2^* - \dot{y}_2) + \lambda_{20}(y_2^* - y_2) \quad (35)$$

where y_1^*, y_2^*, and $\dot{y}_2^*$ are the desired system references. By making, $e_1 = y_1^* - y_1$ and $e_2 = y_2^* - y_2$ the following error dynamics can be formulated from (33)–(35):

$$\dot{e}_1 + \lambda_{10}e_1 = 0 \quad (36)$$

$$\ddot{e}_2 + \lambda_{21}\dot{e}_2 + \lambda_{20}e_2 = 0 \quad (37)$$

which are stable if the gains λ_{10}, λ_{20}, and λ_{21} are greater than zero [25].

In order to have an exact idea of the controller complexity, the control inputs of (32) can be formulated separately as

$$u_1 = L \cdot \left[\frac{1}{L}v_{gq} - \frac{R}{L}i_q - \omega i_d - \gamma_1\right] \quad (38)$$

$$u_2 = \frac{2LCv_{\rm dc}}{3v_{gd}} \cdot \left[\frac{3v_{gd}}{2Cv_{\rm dc}}\left(\frac{v_{gd}}{L} - \frac{R}{L}i_d + \omega i_q\right) - \frac{3v_{gd}i_d}{2Cv_{\rm dc}^2}\left(\frac{3(v_{gd}i_d)}{2Cv_{\rm dc}} - \frac{i_2}{C}\right) - \frac{\dot{i}_2}{C} - \gamma_2\right]. \quad (39)$$

It is worth noting that this controller has been previously reported in [21]. As can be seen, (38) can be implemented in an analog or digital controller, but (39), which linearizes the dc-link voltage, is too complex to implement even for the most advanced digital signal processors. This final relation involves many complex operations such as quadratic terms and divisions, and the sensing of the dc-link current i_2 and its time derivative.

To overcome this drawback, a simple alternative controller based on sliding mode control [26] is proposed in Section III. This controller input–output linearizes the system and can be implemented with a digital or an analog approach.

IV. Sliding Mode Input–Output Feedback Linearization Controller

A. Sliding Mode Controller

In this system, the vector relative degree is $\boldsymbol{r} = (1, 2)$, which coincides with the system order $n = 3$ [27]. The objective is to design an equilibrium surface so that the state trajectories of the

system have the desired behavior when restricted to the surface. In the present case, $S = [s_1, s_2]^T$. Since the relative degree is $r_1 = 1$ for the input y_1 and $r_1 = 2$ for the input y_2, we adopt the following surfaces with the errors of the indirect component current and the dc-link voltage:

$$s_1 = e_1 + \lambda_{10} \int e_1 d\tau \tag{40}$$

$$s_2 = \dot{e}_2 + \lambda_{21} e_2 + \lambda_{20} \int e_2 d\tau \tag{41}$$

where $e_1 = y_1^* - y_1$, $e_2 = y_2^* - y_2$, λ_{10}, λ_{20}, and λ_{21} are positive constants, and $y_1 = i_q$, $y_1^* = i_q^*$, $y_2 = v_{\rm dc}$, and $y_2^* = v_{\rm dc}^*$. If the system states operate on the surface, then $s_1 = s_2 = 0$ and $\dot{s}_1 = \dot{s}_2 = 0$. Substituting (40) and (41) into $\dot{s}_1 = \dot{s}_2 = 0$ yields

$$\dot{e}_1 = -\lambda_{10} e_1 \tag{42}$$

$$\ddot{e}_2 = -\lambda_{21} \dot{e}_2 - \lambda_{20} e_2. \tag{43}$$

These last first and second order equations, (42) and (43), ensure that the system states (i_q and $v_{\rm dc}$) will exponentially converge towards the reference values when they are kept on the sliding surface $S = 0$. The equivalent control concept of a sliding surface is the continuous control that allows for the maintenance of the state trajectory on the sliding surface $S = \dot{S} = 0$. We can obtain the equivalent control from (40) and (41)

$$\begin{aligned} \dot{s}_1 &= \dot{e}_1 + \lambda_{10} e_1 \\ &= \frac{v_{gq}}{L} - \frac{R}{L} i_q - \omega i_d - \frac{1}{L} u_1 + \gamma_1 \end{aligned} \tag{44}$$

$$\begin{aligned} \dot{s}_2 &= \ddot{e}_2 + \lambda_{21} \dot{e}_2 + \lambda_{20} e_2 \\ &= \frac{3 v_{gd}}{2 C v_{\rm dc}} \left(\frac{1}{L} v_{gd} - \frac{R}{L} i_d + \omega i_q - \frac{1}{L} u_2 \right) \\ &\quad - \frac{3 i_d v_{gd}}{2 C v_{\rm dc}^2} \left(\frac{3 (v_{gd} i_d)}{2 C v_{\rm dc}} - \frac{i_2}{C} \right) - \frac{1}{C} \dot{i}_2 + \gamma_2 \end{aligned} \tag{45}$$

where γ_1 and γ_2 coincide with the new inputs of the system defined in (19) and (32), whose expressions are $\gamma_1 = \dot{i}_q^* + \lambda_{10} e_1$, $\gamma_2 = \ddot{v}_{\rm dc}^* + \lambda_{21} \dot{e}_2 + \lambda_{20} e_2$. Finally, the equivalent control is obtained by making $\dot{s}_1 = \dot{s}_2 = 0$, so

$$u_{1eq} = L \cdot \left[\frac{v_{gq}}{L} - \frac{R}{L} i_q - \omega i_d - \gamma_1 \right] \tag{46}$$

$$\begin{aligned} u_{2eq} = \frac{2 L C v_{\rm dc}}{3 v_{gd}} \cdot \Bigg[& \frac{3 v_{gd}}{2 C v_{\rm dc}} \left(\frac{v_{gd}}{L} - \frac{R}{L} i_d + \omega i_q \right) \\ & - \frac{3 v_{gd} i_d}{2 C v_{\rm dc}^2} \left(\frac{3 (v_{gd} i_d)}{2 C v_{\rm dc}} - \frac{i_2}{C} \right) - \frac{\dot{i}_2}{C} - \gamma_2 \Bigg]. \end{aligned} \tag{47}$$

It is interesting to note that the obtained equivalent control is the same as the ones obtained in (38) and (39). Now, in order to drive the state variables to the sliding surface $s_1 = s_2 = 0$, the following control laws are defined:

$$u_1 = u_{1eq} + u_{1s} = u_{1eq} + k_1 sign(s_1) \tag{48}$$

$$u_2 = u_{2eq} + u_{2s} = u_{2eq} + k_2 sign(s_2) \tag{49}$$

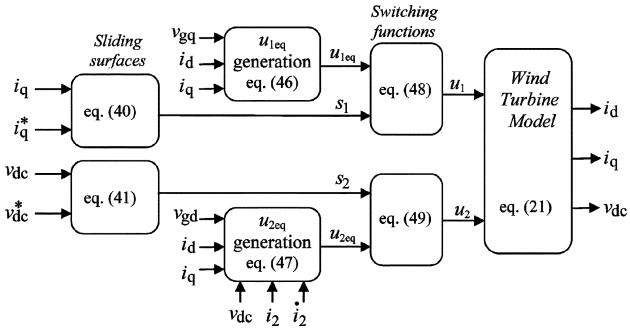

Fig. 5. Block diagram of the input–output feedback linearization sliding mode controller.

where $k_1 > 0$, $k_2 > 0$, and u_{1s} and u_{2s} are switching functions that ensure that the state trajectories are kept on the sliding surfaces. At this time, the reaching law can be derived by substituting (48) into (44) and (49) in (45), which gives

$$\dot{s}_1 = -k_1 sign(s_1) \tag{50}$$

$$\dot{s}_2 = -k_2 sign(s_2). \tag{51}$$

Now, the stability of the sliding mode control can be tested using Lyapunov's function

$$V = \frac{1}{2} S^T S \tag{52}$$

whose time derivative is

$$\dot{V} = S^T \dot{S} = -k_1 |s_1| - k_2 |s_2|. \tag{53}$$

As a result, Lyapunov's function is negative definite, the control system is stable and the system states will converge towards the sliding mode surface in the whole phase space.

Comparing expression (46) with (38) and (47) with (39) we realize that, for the moment, an alternative sliding mode controller has been designed, which input–output linearizes the system. Fig. 5 shows a block diagram of this controller. However, from the point of view of the control complexity no improvement has been made. We still have the same complex expressions and mathematical operations to obtain the control actions. Moreover, we have two extra control surfaces and switching functions (48) and (49).

B. Practical Approach

A different approach can be taken if we put our attention on the equivalent control concept of the sliding mode surface obtained in (46) and (47). The idea is to overcome the controller's complexity by first assigning a switching function to each sliding surface of the form

$$u_{i_{SW}} = \begin{cases} u_{i_{\max}}^+ & \text{if } s_i > 0 \\ u_{i_{\min}}^- & \text{if } s_i \le 0 \end{cases} \tag{54}$$

where $u_{i_{\max}}^+ > u_{i_{\min}}^-$, and $i = 1, 2$ [28]. With these switching functions, when the sliding regime is achieved, the equivalent control of the system is the same as the one obtained in (46) and (47) since the sliding surfaces defined in (40) and (41) had not been modified. The equivalent control can be derived from (54)

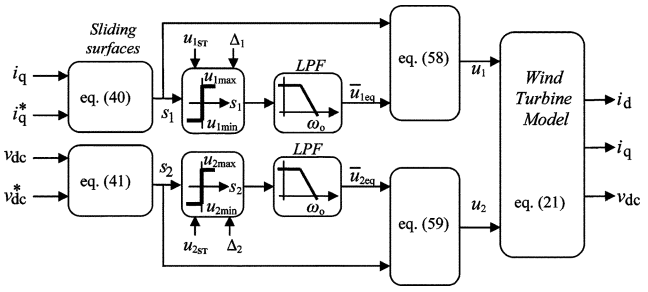

Fig. 6. Block diagram of the simplified sliding-mode controller.

by just averaging the fast discontinuous switching by a simple low-pass filter such as

$$\bar{u}_{i_{eq}} \cong \langle u_{i_{SW}} \rangle = \frac{\omega_o}{p+\omega_o} u_{i_{SW}} \tag{55}$$

where ω_o is the cut-off frequency of the filter and p is the Laplace operator. This filter achieves the equivalent control and, at the same time, reduces the system chattering. However, it introduces an extra time delay in the control system. For this reason, the selection of the cut-off frequency should be neither too low in order to avoid the delay effect on the system dynamics, nor too high in order to avoid excessive chattering in the system states. On the other hand, the chattering of the system can be reduced even more if the switching gains $u^+_{1\max}$, $u^-_{1\min}$, $u^+_{2\max}$, and $u^-_{2\min}$ are chosen around the stationary state of the control inputs, $u_{1_{ST}}$ and $u_{2_{ST}}$, of the system. The steady state of u_1 and u_2 can be derived from (21) as

$$u_{1_{ST}} = v_{gq} - L\omega \frac{2v_{\rm dc}}{3v_{gd}} i_2 - Ri_q \tag{56}$$

$$u_{2_{ST}} = v_{gd} - R \frac{2v_{\rm dc}}{3v_{gd}} i_2 + L\omega i_q. \tag{57}$$

Then, the switching amplitudes can be designed to assure stabilization of the system outputs y_i (i =1, 2) for any constant operating point ($v^*_{\rm dc}$ and i^*_q). The values $u^+_{i_{\max}}$ and $u^-_{i_{\min}}$ can be simply chosen as $u^+_{i_{\max}} = u_{i_{ST}} + \Delta_i$ and $u^-_{i_{\max}} = u_{i_{ST}} - \Delta_i$ (i =1, 2), where Δ_i is a constant value designed to assure the system stabilization around the operating point. Note that the system chattering now is related with the magnitude of Δ_i. Larger Δ_i values are related to faster variations of the output y_i and to bigger system disturbances that may be compensated, but to higher chattering levels. In consequence, Δ_i should be high enough to meet the system requirements, perturbations and parameter variations.

Finally, the same input functions (48) and (49) have been used, but substituting $u_{1_{eq}}$ by $\bar{u}_{1_{eq}}$ and $u_{2_{eq}}$ by $\bar{u}_{3_{eq}}$

$$u_1 = \bar{u}_{1eq} + k_1 sign(s_1) \tag{58}$$

$$u_2 = \bar{u}_{2eq} + k_2 sign(s_2) \tag{59}$$

where the terms k_1 and k_2 guarantee the existence of the sliding mode in the surface.

As in (34) and (35), a desired dynamic can be imposed on the system by the coefficients λ_{10}, λ_{20}, and λ_{21} of the sliding surfaces s_1 and s_2. By making $e_q = i^*_q - i_q$ and $e_{\rm dc} = v^*_{\rm dc} - v_{\rm dc}$, the following tracking error dynamics can be formulated:

$$\dot{e}_q + \lambda_{10} e_q = 0 \tag{60}$$

$$\ddot{e}_{\rm dc} + \lambda_{21}\dot{e}_{\rm dc} + \lambda_{20} e_{\rm dc} = 0 \tag{61}$$

which are stable if the gains λ_{10}, λ_{20}, and λ_{21} are greater than zero. Therefore, the same linear closed-loop dynamics can be obtained by using a very simple control implementation (see Fig. 6).

V. Simulation Results

The sliding mode feedback linearization controller proposed in the previous section, (40) and (41) and (54)–(59) (see Fig. 6), was applied to the system model of the grid-side VSC and simulated by using Matlab/Simulink software. Assuming that i_q is regulated around zero, a maximum current perturbation of -1000 A on i_2, and a maximum voltage dip of 15% from nominal, the stationary values of (56) and (57) can be approximated to $u_{1_{ST}} \approx v_{gq}$ and $u_{2_{ST}} \approx v_{gd}$, respectively. The bounds for the other terms of (56) and (57) goes from 20 V–135 V and from 2–14 V, respectively, for nominal grid voltage and for 15% voltage dip. This variations can be compensated by choosing $\Delta_1 = 160$ V and $\Delta_2 = 50$ V to ensure the convergence of the system outputs to the reference set points. At the same time, a cut-off frequency of $\omega_o = 2\pi$ 2200 rad/s for the low pass filters in (55) was selected in order not to affect the system dynamics. The constants k_1 and k_2 in (58) and (59) were set to $k_1 = k_2 =$ 10 in order to ensure the existence of the sliding surfaces.

Several simulations were carried out in order to examine the system performance under different controller parameters. In each case, the operating grid voltage was maintained constant at the chosen level. The parameter λ_{10} in (40) was set to 600 rad/s in order to ensure an exponential convergence on the sliding surface s_1, while the parameters λ_{20} and λ_{21} in (41) vary in order to check the transient behavior of the grid-side and dc-link-side variables of the VSC.

Fig. 7(a) depicts the transient response of the i_1 dc-link current for 15% of the grid voltage and -1000 A transient perturbation on i_2. In this figure, λ_{20} and λ_{21} were selected in order to impose a double-pole dynamic behavior as $(p+\lambda)^2$ (p is the Laplace operator, $\lambda_{21} = 2\lambda$, and $\lambda_{20} = \lambda^2$) with values: $\lambda =$ 10 rad/s for transient marked as ***ra***, $\lambda = 50$ rad/s for transient ***rb***, $\lambda = 100$ rad/s for transient ***rc***, and $\lambda = 150$ rad/s for transient ***rd***. Note that exponential dynamic behavior agrees with the imposed dynamics. On the other hand, Fig. 7(b) depicts the transient response under the same conditions as Fig. 7(a), but for parameters that lead to complex-conjugate roots. The transient responses marked as ***ra***, ***rb***, and ***rc***, in Fig. 7(b), correspond to roots $\lambda = -\sigma \pm j\omega_c$ with a real part $\sigma = 50$ rad/s and imaginary parts $\omega_c = 100$ rad/s, $\omega_c = 200$ rad/s, and $\omega_c = 300$ rad/s, respectively. Note that the damped oscillatory dynamics depicted in this figure follows the imposed dynamics.

Fig. 8 depicts the transient behavior on the link current i_1, the dc-link voltage $v_{\rm dc}$, and the indirect component current i_q to the -1000 A perturbation on i_2 and for grid voltages 15% and 100% of nominal. These responses were obtained for a double-pole dynamic behavior $(p+\lambda)^2$ imposed on λ_{20} and λ_{21} with $\lambda =$ 25 rad/s. Note that an excellent transient response is achieved in comparison with the results of the conventional linear controller shown in Fig. 3. In fact, both lower current and voltage overshoots and smaller recovery time are obtained. Moreover, i_q current is kept around zero without transient.

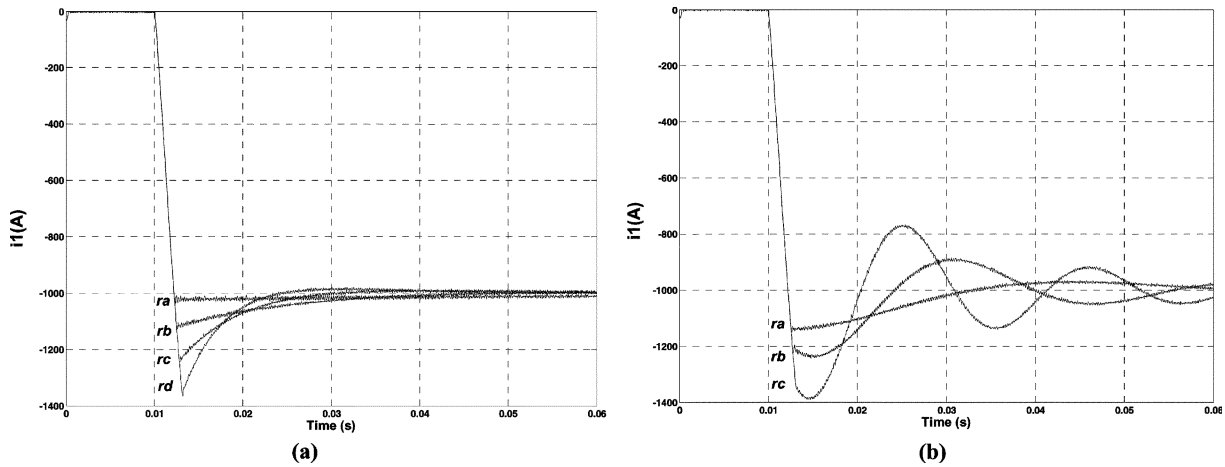

Fig. 7. Dc-link current i_1 response to a -1000 A perturbation on i_2 current with 15% of nominal grid voltage. (a) Responses marked as $\boldsymbol{ra}$, $\boldsymbol{rb}$, $\boldsymbol{rc}$, and $\boldsymbol{rd}$ correspond to a double-pole behavior imposed with λ_{20} and λ_{21} ($\lambda_{21} = 2\lambda$ and $\lambda_{20} = \lambda^2$, $\lambda = 10$ rad/s for $\boldsymbol{ra}$, $\lambda = 50$ rad/s for $\boldsymbol{rb}$, $\lambda = 100$ rad/s for $\boldsymbol{rc}$, and $\lambda = 150$ rad/s for $\boldsymbol{rd}$). (b) Responses marked as $\boldsymbol{ra}$, $\boldsymbol{rb}$, and $\boldsymbol{rc}$ correspond to complex-conjugate roots imposed with λ_{20} and λ_{21} ($\lambda = -\sigma \pm j\omega_c$, $\sigma = 50$ rad/s for $\boldsymbol{ra}$, $\boldsymbol{rb}$, and $\boldsymbol{rc}$, $\omega_c = 100$ rad/s for $\boldsymbol{ra}$, $\omega_c = 200$ rad/s for $\boldsymbol{rb}$, $\omega_c = 300$ rad/s for $\boldsymbol{rc}$).

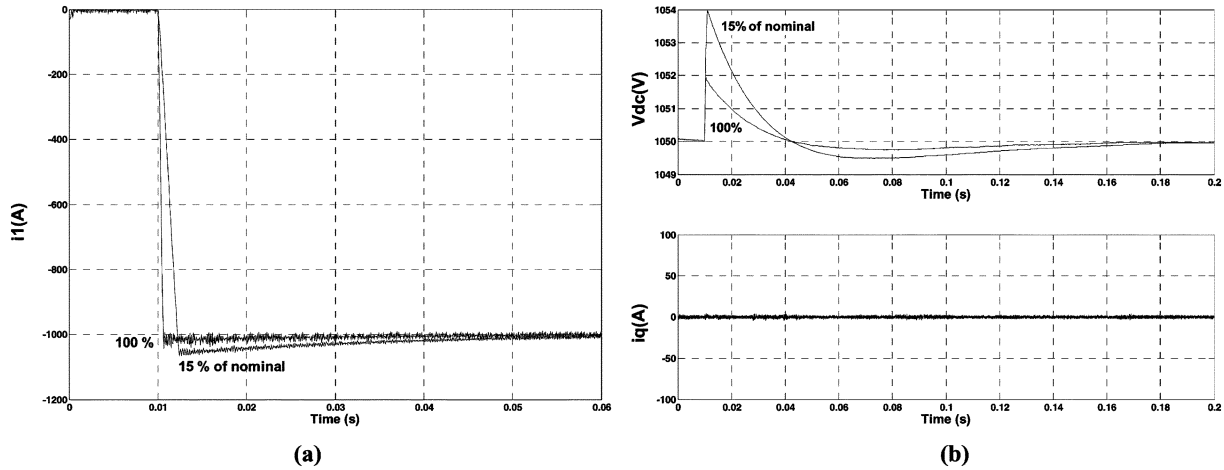

Fig. 8. Transient response to a -1000 A perturbation on i_2 and under 15% and 100% of nominal grid voltage. (a) link current i_1. (b) Upper: dc-link voltage $v_{\rm dc}$, lower: i_q current.

In Fig. 9(a) the response of the sliding surfaces are depicted. The effect of the perturbation on the current i_2 can be noticed as a short but great peak on the surface s_2. At this instant, the controller reacts by forcing the system states towards the sliding surfaces. Fig. 8(b) shows the transient response on the grid side VSC i_d peak current, plotted in pu. Note that the sliding mode feedback linearization controller achieves a strong reduction in the transient peaks, in comparison with results shown in Fig. 4. It can be seen that as the grid voltage reduces, from 100% to 15% of its nominal level, the i_d peak current of the grid-side VSC changes by less than 1.2%. However, as it is shown in Fig. 5(a), these results depend on the dynamic imposed to the system, a double-pole with $\lambda = 25$ rad/s in this case. Thus, further peak reduction can be achieved by reducing this parameter or by choosing a better dynamic response to the system.

In order to compare the controller performance, the nonlinear controller proposed in [21] has been simulated under the same conditions as the proposed controller. Fig. 10 shows the transient response of the proposed controller (NLSC) and of the controller reported in [21] (NLC) for 15% of the grid voltage and -1000 A transient perturbation on i_2. The responses marked as $\boldsymbol{ra}$ and $\boldsymbol{rb}$ for the proposed controller correspond to a double-pole dynamic behavior with values $\lambda = 25$ rad/s and $\lambda = 75$ rad/s, respectively. Note that the response of both controllers are similar and depend mainly on the imposed dynamics.

The sliding mode control has the inherent property of robustness against parametric uncertainty and external disturbances. In order to examine the effect of plant model mismatch, a series of simulations were performed for model mismatches on L, R, and C in the range of $\pm 30\%$. These mismatches can be produced in the measurements of R and L made between the grid-side VSC converter terminals and the high voltage terminals of the grid-connected transformer. Fig. 11 shows the effect of these mismatches for each model parameter. These simulations were made for a grid voltage level of 15% nominal. Moreover, these simulations have been also performed for the controlled reported in [21] in order to compare the results with the proposed controller. The results show that the impact of the mismatch on the peak current levels is less than 1.76% around nominal for the proposed controller and less than 4.47% around nominal for the controller reported in [21]. Although these mismatches were realized among one of the parameters while the others were maintained at the nominal value, simulations in the worst case of mismatch over all these parameters were per-

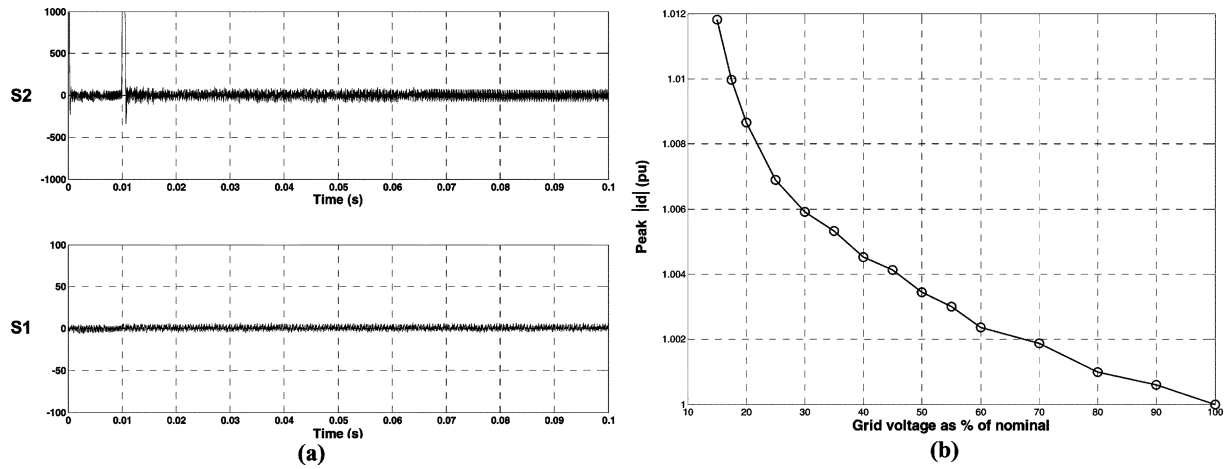

Fig. 9. (a) Response of the sliding surfaces s_1 (lower) and s_2 (upper). (b) Peak i_d magnitude response to a -1000 A perturbation on the i_2 dc-link current and for decreasing levels of grid voltage (from 100% to 15% nominal).

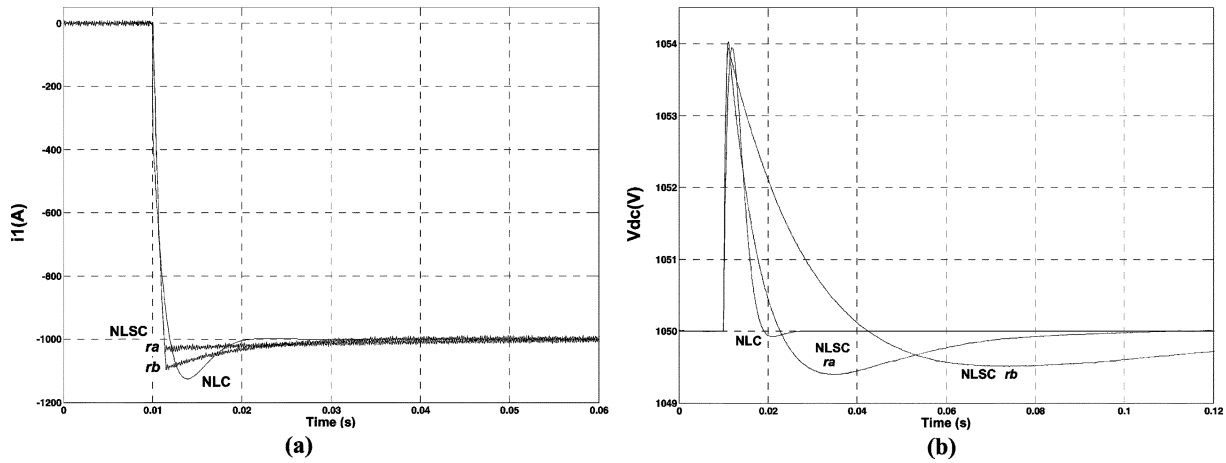

Fig. 10. Transient response to a -1000 A perturbation on i_2 and under 15% of nominal grid voltage for the proposed (NLSC) and the reported one in [21] (NLC). The responses marked as ***ra*** and ***rb*** correspond to a double-pole behavior imposed with λ_{20} and λ_{21} ($\lambda_{21} = 2\lambda$ and $\lambda_{20} = \lambda^2$, $\lambda = 25$ rad/s for ***ra*** and $\lambda = 75$ rad/s for ***rb***): (a) dc-link current i_1 and (b) dc-link voltage $v_{\rm dc}$.

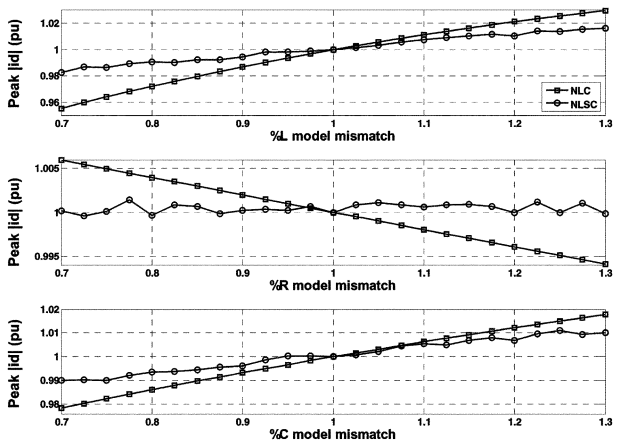

Fig. 11. Peak i_d response to a -1000 A perturbation on the i_2 current at 15% nominal grid voltage for model mismatches in the range of $\pm 30\%$: L (upper), R (middle), and C (lower). The NLC plot is from the controller proposed in [21] and NLSC plot is from the proposed controller with a double-pole dynamics $\lambda = 75$ rad/s.

formed, giving similar results with peak current levels below 2.89% nominal for the proposed controller and below 7.64% nominal for the controller reported in [21].

The results reported in this section show the interesting properties of the proposed nonlinear controller, i.e., linear closed loop dynamics, fast transient response, small current and voltage overshoots, and high robustness to plant model mismatches. Therefore, the proposed controller seems to be an attractive alternative solution to improve the ride-through capability of wind turbines based on DDSGs.

VI. Conclusion

This paper proposes the application of feedback linearization theory to wind turbines based on direct drive synchronous generators via a sliding mode control approach. The proposed controller is suitable to improve the ride-through capability of these turbines, since they must operate and stay connected to the grid at voltage levels far below nominal as stipulated by today's grid codes. In the first part of the paper, the system behavior using linear PI controllers was analyzed. These controllers are usually designed around a nominal operating point, which leads to increasing current levels in the wind turbine converter at grid faults that can result in converter damage.

The application of a feedback linearization controller was studied in order to overcome the linear controller's limitations. However, the proposed controller was too difficult to implement,

since it involves a great number of terms, divisions, quadratic terms and the sensing of one of the dc-link currents and its time derivative. To overcome this obstacle, a sliding mode controller has been proposed, which simplifies further the controller structure. The sliding controller uses a low pass filter to reduce the system chattering and to obtain the system equivalent control.

The paper demonstrates that the proposed design reduces the chattering of the system to acceptable levels while still maintaining good tracking on the reference variables. Furthermore, since the system has been linearized, a proper dynamic response can be imposed on the system only by modifying the sliding surface coefficients.

Finally, a series of simulations were carried out in order to test the performance of the proposed controller. The obtained results validate the proposed control approach and demonstrate that it is able to improve the ride-through capability of wind turbines. The huge transients produced by grid faults when the linear controllers are used are reduced significantly. Furthermore, a series of simulations were also performed in order to test the controller behavior in the presence of model mismatches in the range of $\pm 30\%$ of the nominal values. The reported results show that the sliding mode control has high robustness against parametric uncertainty, causing small deviations in the peak current levels produced during network faults.

REFERENCES

[1] J. Ekanayake and N. Jenkins, "Comparison of the response of doubly fed and fixed-speed induction generator wind turbines to changes in network frequency," *IEEE Trans. Energy Conver.*, vol. 19, no. 4, pp. 800–802, Dec. 2004.

[2] L. Holdsworth, X. G. Wu, J. B. Ekanayake, and N. Jenkins, "Comparison of fixed speed and doubly fed induction wind turbines during power system disturbances," *Proc. Inst. Elect. Eng.*, vol. 150, no. 3, pp. 343–352, May 2003.

[3] E.ON Netz GmbH, "Grid Code for High and Extra High Voltage 2006 [Online]. Available: http://www.eon-netz.com/Ressources/downloads/ENENARHS2006eng.pdf

[4] "Royal Decree," Ministerio de Economía y Hacienda, Real Decreto 436/2004, May 27, 2004, pp. 13217–13228.

[5] "Specifications for Connecting Wind Farms to the Transmission Network," Eltra Corp., 2004 [Online]. Available: http://www.eltra.dk

[6] S. Seman, J. Niiranen, and A. Arkkio, "Ride-through analysis of doubly fed induction wind-power generator under unsymmetrical network disturbance," *IEEE Trans. Power Syst.*, vol. 21, no. 4, pp. 1782–1789, Nov. 2006.

[7] F. M. Hughes, O. Anaya-Lara, N. Jenkins, and G. Strbac, "A power system stabilizer for dfig-based wind generation," *IEEE Trans. Power Syst.*, vol. 21, no. 2, pp. 763–772, May 2006.

[8] G. Saccomando, J. Svensson, and A. Sannino, "Improving voltage disturbance rejection for variable-speed wind turbines," *IEEE Trans. Energy Conversion*, vol. 17, no. 3, pp. 422–428, Sep. 2002.

[9] H. Polinder, S. W. H. d. Haan, and R. Dubois, "Basic operation principles and electrical conversion systems of wind turbines," *EPE J.*, vol. 15, no. 4, pp. 43–50, Dec. 2005.

[10] F. Blaabjerg, R. Teodorescu, M. Liserre, and A. V. Timbus, "Overview of control and grid synchronization for distributed power generation systems," *IEEE Trans. Ind. Electron.*, vol. 53, no. 5, pp. 1398–1409, Oct. 2006.

[11] M. Liserre, R. Teodorescu, and F. Blaabjerg, "Stability of photovoltaic and wind turbine grid-connected inverters for a large set of grid impedance values," *IEEE Trans. Power Electron.*, vol. 21, no. 1, pp. 263–272, Jan. 2006.

[12] N. R. Ullah, T. Thiringer, and D. Karlsson, "Voltage and transient stability support by wind farms complying with the E.ON netz grid code," *IEEE Trans. Power Syst.*, vol. 22, no. 4, pp. 1647–1656, Nov. 2007.

[13] J. L. Durán-G\sigma mez, P. N. Enjeti, and B. O. Woo, "Effect of voltage sags on adjustable-speed drives: A critical evaluation and an approach to improve performance," *IEEE Trans. Ind. Appl.*, vol. 35, no. 6, pp. 1440–1448, Nov./Dec. 1999.

[14] A. Causebrook, D. J. Atkinson, and A. G. Jack, "Fault ride-through of large wind farms using series dynamic braking resistors," *IEEE Trans. Power Syst.*, vol. 22, no. 3, pp. 966–975, Aug. 2007.

[15] T. D. Vrionis, X. I. Koutiva, N. A. Vovos, and G. B. Giannakopoulos, "Control of an hvdc link connecting a wind farm to the grid for fault ride-through enhancement," *IEEE Trans. Power Syst.*, vol. 22, no. 4, pp. 2039–2047, Nov. 2007.

[16] T. Thringer, "Power quality measurements performed on a low-voltage grid equipped with two wind turbines," *IEEE Trans. Energy Conversion*, vol. 11, no. 3, pp. 601–606, Sep. 1996.

[17] B. Xie, B. Fox, and D. Flynn, "Study of fault ride-through for DFIG based wind turbines," in *Proc. IEEE Int. Conf. Elect. Utility Dereg., Restr. Power Tech. (DRPT2004)*, Apr. 2004, pp. 401–416.

[18] C. Chompoo-inwai, C. Yingvivatanapong, K. Methaprayoon, and W.-J. Lee, "Reactive compensation techniques to improve ride-through capability of wind turbine during disturbance," *IEEE Trans. Ind. Appl.*, vol. 41, no. 3, pp. 666–672, May/Jun. 2005.

[19] J. Morren and S. W. H. d. Han, "Ridethrough of wind turbines with doubly-fed induction generator during a voltage dip," *IEEE Trans. Energy Conversion*, vol. 20, no. 2, pp. 435–441, Jun. 2005.

[20] P. Rodriguez, A. V. Timbus, R. Teodorescu, M. Liserre, and F. Blaabjerg, "Flexible active power control of distributed power generation systems during grid faults," *IEEE Trans. Power Electron.*, vol. 54, no. 5, pp. 2583–2592, Oct. 2007.

[21] A. Mullane, G. Lightbody, and R. Yacamini, "Wind-turbine fault ride-through enhancement," *IEEE Trans. Power Syst.*, vol. 20, no. 4, pp. 1929–1937, Nov. 2005.

[22] P. Kundur, *Power System Stability and Control*. New York: McGraw-Hill, 1994.

[23] L. Malesani and L. Rossetto, "AC/DC/AC PWM converter with reduced energy storage in the DC link," *IEEE Trans. Ind. Appl.*, vol. 31, no. 2, pp. 287–292, Mar./Apr. 1995.

[24] T. A. Belli, R. P. O'Leary, and E. H. Camm, "Evaluating capacitor-switching devices for preventing nuisance tripping of adjustable-speed drives due to voltage magnification," *IEEE Trans. Power Delivery*, vol. 11, no. 3, pp. 1373–1378, Jul. 1996.

[25] J. J. E. Slotine and W. Li, *Applied Nonlinear Control*. Englewood Cliffs, NJ: Prentice-Hall, 1991.

[26] V. Utkin, *Sliding Modes In Control And Optimization*. New York: Springer-Verlag, 1992.

[27] J. Y. Yung, W. Gao, and J. C. Hung, "Variable structure control: A survey," *IEEE Trans. Ind. Electron.*, vol. 40, no. 1, pp. 2–22, Feb. 1993.

[28] I. Alberto, *Nonlinear Control Systems*, 3rd ed. New York: Springer Verlag.

José Matas received the B.S., M.S., and Ph.D. degrees in telecommunications engineering from the Technical University of Catalonia, Barcelona, Spain, in 1988, 1996, and 2003, respectively.

From 1988 to 1990, he was an Engineer of a consumer electronics company. Since 1990, he has been an Associate Professor in the Department of Electronic Engineering, Technical University of Catalonia, Vilanova i la Geltrú, Spain. His research interests include power-factor-correction circuits, active power filters, uninterruptible power systems, distributed power systems, nonlinear control, and renewable energy systems.

Miguel Castilla received the M.S. and Ph.D. degrees in telecommunications engineering from the Technical University of Catalonia, Barcelona, Spain, in 1995 and 1998, respectively.

Since 2002, he has been an Associate Professor in the Department of Electronic Engineering, Technical University of Catalonia, Vilanova i la Geltrú, Spain, where he teaches analog circuits and power electronics. His research interests are in the areas of modeling, simulation, and control of dc-to-dc power converters, high-power-factor rectifiers, and dc-to-ac converters.

Josep M. Guerrero (S'01–M'03) received the B.S. degree in telecommunications engineering, the M.S. degree in electronics engineering, and the Ph.D. degree in power electronics from the Technical University of Catalonia, Barcelona, Spain, in 1997, 2000, and 2003, respectively.

From 1998 to 2004, he was an Assistant Professor in the Department of Automatic Control Systems and Computer Engineering, Technical University of Catalonia. In 2004, he became a Senior Lecturer at the same university, where he teaches courses on digital signal processing, control theory, and microprocessors. Since 2004, he has been responsible for the Sustainable Distributed Generation and Renewable Energy Research Group, Escola Industrial de Barcelona. His research interests include DSP/FPGA-based control, uninterruptible power systems, inverters for photovoltaic applications, and wind energy conversion in microgrids.

Dr. Guerrero is an Associate Editor of the IEEE TRANSACTIONS ON INDUSTRIAL ELECTRONICS. He is a Guest Editor of the Special Issue of the IEEE TRANSACTIONS ON POWER ELECTRONICS "Power Electronics for Wind Energy" and the Special Section of the IEEE TRANSACTIONS ON INDUSTRIAL ELECTRONICS "Uninterruptible Power Supply (UPS) Systems." He has organized and chaired sessions at several IEEE IECON, APEC, and PESC Conferences.

Luis García de Vicuña received the M.S. and Ph.D. degrees in telecommunications engineering from the Universitat Politècnica de Catalunya, Barcelona, Spain, in 1980 and 1990, respectively, and the Dr.Sci. degree from the Université Paul Sabatier, Toulouse, France, in 1992.

From 1980 to 1982, he was an Engineer with control applications company. He is currently an Associate Professor in the Departament d'Enginyeria de Electrònica, Universitat Politècnica de Catalunya, where he teaches power electronics. His research interests include power electronics modeling, simulation and control, active power filtering, and high-power-factor ac–dc conversion.

Jaume Miret (M'98) received the B.S. degree in telecommunications, the M.S. degree in electronics, and the Ph.D. degree in electronics from the Technical University of Catalonia, Barcelona, Spain, in 1992, 1999, and 2005, respectively.

Since 1993, he has been an Assistant Professor in the Department of Electronic Engineering, Technical University of Catalonia, Vilanova i la Geltrú, Spain, where he teaches courses on digital design and circuit theory. His research interests include dc-to-ac converters, active power filters, and digital control.